Neurobiology of Disease 200 (2024) 106625

Contents lists available at ScienceDirect

Neurobiology of Disease

journal homepage: www.elsevier.com/locate/ynbdi

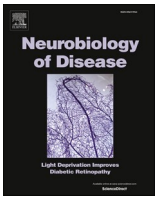

Disease-associated mutations in C-terminus of HSP70 interacting protein (CHIP) impair its ability to negatively regulate mitophagy

Rebecca Earnshaw [a,b], Yu Tong Zhang [a,b], Gregory Heymann [a,b], Kazuko Fujisawa [a], Sarah Hui [a,b], Minesh Kapadia [a], Lorraine V. Kalia [a,b,c,d,1], Suneil K. Kalia [a,b,d,e,*,1]

[a] Krembil Research Institute, Toronto Western Hospital, University Health Network, 60 Leonard Avenue, Toronto, ON M5T 0S8, Canada
[b] Department of Laboratory Medicine and Pathobiology, University of Toronto, 1 King's College Circle, Toronto, ON M5S 1A8, Canada
[c] Division of Neurology, Department of Medicine, University of Toronto, 399 Bathurst Street, Toronto, ON M5T 2S8, Canada
[d] CRANIA, University Health Network, 550 University Avenue, Toronto, ON M5G 2A2, Canada
[e] Division of Neurosurgery, Department of Surgery, University of Toronto, 399 Bathurst Street, Toronto M5T 2S8, ON, Canada

ARTICLE INFO

Keywords:
Mitophagy
STUB1
Neurodegeneration
SCA48
Ataxia

ABSTRACT

C-terminus of HSP70 interacting protein (CHIP) is an E3 ubiquitin ligase and HSP70 cochaperone. Mutations in the CHIP encoding gene are the cause of two neurodegenerative conditions: spinocerebellar ataxia autosomal dominant type 48 (SCA48) and autosomal recessive type 16 (SCAR16). The mechanisms underlying CHIP-associated diseases are currently unknown. Mitochondrial dysfunction, specifically dysfunction in mitochondrial autophagy (mitophagy), is increasingly implicated in neurodegenerative diseases and loss of CHIP has been demonstrated to result in mitochondrial dysfunction in multiple animal models, although how CHIP is involved in mitophagy regulation has been previously unknown. Here, we demonstrate that CHIP acts as a negative regulator of the PTEN-induced kinase 1 (PINK1)/Parkin-mediated mitophagy pathway, promoting the degradation of PINK1, impairing Parkin translocation to the mitochondria, and suppressing mitophagy in response to mitochondrial stress. We also show that loss of CHIP enhances neuronal mitophagy in a PINK1 and Parkin dependent manner in *Caenorhabditis elegans*. Furthermore, we find that multiple disease-associated mutations in CHIP dysregulate mitophagy both *in vitro* and *in vivo* in *C. elegans* neurons, a finding which could implicate mitophagy dysregulation in CHIP-associated diseases.

1. Introduction

Mutations in the STIP1 homology and Ubox containing 1 (*STUB1*) gene, are the cause of two incurable neurodegenerative conditions: spinocerebellar ataxia autosomal dominant type 48 (SCA48; OMIM#618093) (Genis et al., 2018; Michele et al., 2019; Lieto et al., 2020; Palvadeau et al., 2020; Chen et al., 2020; Mol et al., 2020; Roux et al., 2020; Ravel et al., 2021; Mengel et al., 2021; Pakdaman et al., 2017; Chen et al., 2021; Pakdaman et al., 2021; Magri et al., 2022; Umano et al., 2022; Reis et al., 2022; Radziwonik et al., 2022; Barbier et al., 2022; Saito et al., 2022) and spinocerebellar ataxia autosomal recessive type 16 (SCAR16; OMIM#615768) (Roux et al., 2020; Ravel et al., 2021; Shi et al., 2013; Shi et al., 2014; Synofzik et al., 2014; Heimdal et al., 2014; Depondt et al., 2014; Cordoba et al., 2014;

Abbreviations: C. elegans, *Caenorhabditis elegans*; CCCP, Carbonyl cyanide *m*-chlorophenylhydrazone; CHIP, C-terminus of HSP70 interacting protein; CHN-1, C-terminus of HSP70 interacting protein (*C. elegans*); CRISPR, Clustered regularly interspaced short palindromic repeats; DCT-1, DAF-16/FOXO-controlled germline tumor affecting-1; del, Deletion; DMSO, Dimethyl sulfoxide; EV, Empty vector; fs, Frameshift; HSP70, Heat shock protein 70; LC3, Microtubule-associated protein 1 light chain 3; LGG-1, *C. elegans* LC3 homologue; MEF, Mouse embryonic fibroblast; Mitophagy, Mitochondrial autophagy; mt-Keima, mito-mKeima; mtRosella, Mitochondrially localized Rosella reporter protein; OMM, Outer mitochondrial membrane; PDR-1, Parkinson's disease related-1/Parkin (*C. elegans*); PINK1, PTEN-induced kinase 1; PINK-1, PTEN-induced kinase 1 (*C. elegans*); SCA48, Spinocerebellar ataxia autosomal dominant type 48; SCAR16, Spinocerebellar ataxia autosomal recessive type 16; siCHIP, siRNA targeting CHIP; siNTC, Non-targeting control siRNA; siRNA, Small interfering RNA; STUB1, STIP1 homology and Ubox containing protein 1; TOMM20, Translocase of the outer mitochondrial membrane 20; TOMM-20, Translocase of the outer mitochondrial membrane 20 (*C. elegans*); TPR, Tetratricopeptide repeat region; WT, Wild-type.

* Corresponding author at: Krembil Research Institute, University Health Network, 60 Leonard Avenue, Toronto, ON M5T 0S8, Canada.
E-mail address: Suneil.kalia@utoronto.ca (S.K. Kalia).

[1] Authors contributed equally.

https://doi.org/10.1016/j.nbd.2024.106625
Received 25 January 2024; Received in revised form 5 June 2024; Accepted 31 July 2024
Available online 6 August 2024

Bettencourt et al., 2015; Kawarai et al., 2016; Hayer et al., 2017; Retterer et al., 2016; Coutelier et al., 2017; Gazulla et al., 2018; Turkgenc et al., 2018; Olszewska and Kinsella, 2020; Chiu et al., 2020). Both SCA48 and SCAR16 result in significant degeneration of cerebellar Purkinje neurons and are associated with a high prevalence of ataxia and cognitive impairment as well as a wide range of additional symptoms that vary from one patient to the next (Chen et al., 2020; Mol et al., 2020; Roux et al., 2020; Bettencourt et al., 2015; Mylvaganam et al., 2021).

The *STUB1* gene encodes C-terminus of HSP70 interacting protein (CHIP), a cochaperone and an E3 ubiquitin ligase. CHIP is comprised of an N-terminal tetratricopeptide repeat (TPR) region, which facilitates its interaction with chaperones, including HSP70, an internal coiled-coil domain, and a C-terminal Ubox domain, which mediates its E3 ubiquitin ligase function (Ballinger et al., 1999). Utilizing both its TPR and Ubox domains together, CHIP is capable of ubiquitinating chaperone-bound substrate proteins and targeting them for degradation (Mylvaganam et al., 2021; Ballinger et al., 1999; McDonough and Patterson, 2003). While CHIP is largely described for its role in facilitating the elimination of aberrant proteins, it has also been demonstrated to exert regulatory control over a number of diverse cellular pathways (Mylvaganam et al., 2021).

Despite many CHIP functions being known (Mylvaganam et al., 2021), how mutations in CHIP lead to neurodegeneration is currently unclear. Animals lacking CHIP, which exhibit Purkinje neuron degeneration and ataxia (Shi et al., 2013; Shi et al., 2014; Palubinsky et al., 2015), have mitochondrial dysfunction (Palubinsky et al., 2015; Lizama et al., 2018; Dai et al., 2003; Yoo and Chung, 2018; Schisler et al., 2016) as well as elevated levels of the proteins PTEN-induced kinase 1 (PINK1) and Parkin within their brains (Palubinsky et al., 2015). PINK1 and Parkin are both key regulatory proteins in the PINK1/Parkin mitochondrial autophagy (mitophagy) pathway, a process by which mitochondria are selectively degraded *via* macroautophagy. Proper mitophagy regulation is crucial for cellular health as it facilitates the basal turnover of mitochondria, which is necessary for maintaining a healthy mitochondrial population, and is also responsible for removing damaged or dysfunctional mitochondria (Palikaras et al., 2018). Dysregulation of the PINK1/Parkin-mediated mitophagy pathway is implicated in multiple neurodegenerative diseases including Parkinson's disease (Hsieh et al., 2016; Geisler et al., 2010; Zhang et al., 2010), Alzheimer's disease (Fang et al., 2019; Ye et al., 2015; Martín-Maestro et al., 2016), amyotrophic lateral sclerosis (Rogers et al., 2017; Palomo et al., 2018) and spinocerebellar ataxia type 3 (Harmuth et al., 2022).

In the absence of mitochondrial stress, PINK1, a serine/threonine kinase, is rapidly degraded by the proteasome (Yamano and Youle, 2013). Upon mitochondrial damage or dysfunction, PINK1 is stabilized on the surface of damaged mitochondria and subsequently phosphorylates a number of substrates including the E3 ubiquitin ligase Parkin (Matsuda et al., 2010). Phosphorylation of Parkin by PINK1 leads to Parkin's recruitment to mitochondria where it ubiquitinates several outer mitochondrial membrane (OMM) proteins. Ubiquitinated OMM proteins are recognized by the autophagy receptor protein microtubule-associated protein 1 light chain 3 (LC3) which is fused to an isolated membrane referred to as a phagophore (Youle and Narendra, 2011; Tang et al., 2017; Gegg et al., 2010; Zhang et al., 2012). Following the recognition of mitochondria by LC3, the phagophore extends around the mitochondria, eventually enveloping it in a double membraned vesicle referred to as a phagosome. The phagosome can then fuse with the lysosome, resulting in the mitochondria being degraded by the hydrolytic enzymes and acidic environment present within the lysosomal lumen (Grumati and Dikic, 2018).

While it is known that loss of CHIP induces mitochondrial dysfunction and elevates levels of PINK1 and Parkin, how it promotes mitochondrial dysfunction is currently unclear. We hypothesized that CHIP may be involved in maintaining mitochondrial homeostasis by regulating PINK1/Parkin-mediated mitophagy and that disease-associated mutations in CHIP dysregulate this pathway.

2. Materials and methods

2.1. Cell culture

U2OS cells stably expressing GFP-Parkin or both GFP-Parkin and mito-mKeima were a gift from Dr. Edward Fon and Dr. Matthew Tang and were generated as previously described (Tang et al., 2017; Durcan et al., 2014). U2OS and HEK293T cells were maintained in Dulbecco's Modified Essential Media (Gibco, 11,965–092) supplemented with 10% fetal bovine serum (Sigma, F2442), and 1% penicillin/streptomycin (Gibco, 1,540,062) at 37 °C in 5% CO_2.

2.2. Transfections

For overexpression experiments, cells were plated 24 h prior to all plasmid transfections. Plasmids and Lipofectamine 2000 (Invitrogen, 11,668–019) were diluted in Opti-MEM (Gibco, 31,985–070) according to manufacturer's direction and added to cells in fresh complete media.

The following DNA expression constructs were used: pDONR201 (Invitrogen), pcDNA3.1 (Invitrogen, V79020), pEGFP-C3 (Clontech, V012022), pDEST-FLAG (88), pcDNA3.1-Myc-CHIP (Yamano and Youle, 2013), pEGFP-HSP70 (Addgene plasmid # 15215), pDest-565 (Addgene plasmid # 11520), and pDONR201-CHIP (Kalia et al., 2011).

For knockdown experiments, siRNA was transfected using RNAi MAX Lipofectamine reagent (Invitrogen, 13,778–075) diluted in Opti-MEM according to Manufacturer's instructions. Transfections were performed at the time the cells were plated and incubated for 24 h. After the 24 h incubation, media was replaced with fresh complete media. Cells were assessed 48 h after plating/transfection. siRNAs used were siNTC (ThermoFisher, 4,390,843) sequence undisclosed and siCHIP (ThermoFisher, s195026) sense sequence: 5'-CGCUGGUGGCCGUGUAUUAtt-3'; antisense sequence: antisense: 5'-UAAUACACGGCCACCAGCGgg-3′.

2.3. Mutagenesis

Mutagenesis was performed to generate expression vectors for the I53T and L275Dfs*16 CHIP mutants using the Q5 site-directed Mutagenesis Kit (New England Biolabs, E0554S) according to manufacturer's instructions using the following primers. Primer sequences were generated using the NEB BaseChanger software.

I53T-F: 3′- GGCCGCGCGACCACCCGGAAC.

I53T-R: 3′- GTAGCAGGCCGCCGCCTC.

L275Dfs*16-F: 3'-GACCCAGGAACAGCTCATCCCCAAC.

L275Dfs*16-R: 3′- GGGGCTCCGGGTCACGGG.

Mutagenesis was performed on pDONR201-CHIP and the Gateway LR Clonase II Enzyme mix (Invitrogen, 11791020) was used to move pDONR201-CHIPs into pDEST-FLAG and pDEST-565 backbones according to manufacturer's specifications.

2.4. Parkin translocation

Parkin translocation was performed as previously described (De Snoo et al., 2019). U2OS GFP-Parkin cells were plated in Lab-Tek 2 Chambered Coverglass (ThermoFisher, 154534PK) and transfections were performed as previously described. 48 h post siRNA transfection and 24 h post plasmid transfection, cells were treated with 10 μM (siRNA knockdown experiments) or 20 μM (plasmid overexpression experiments) CCCP (Sigma, C2759) or DMSO (Sigma, D2650) for 1 h. Cells were washed for 5 min with PBS (Sigma, D8537) and fixed with 4% paraformaldehyde for 15 min. Cells were subsequently washed three times and permeabilized with 0.2% TritonX-100 diluted in PBS for 15 min. Cells were then washed again 3 times and then blocked for 1 h at room temperature in 5% bovine serum albumin in PBS. Primary

antibodies diluted in blocking buffer were incubated at 4 °C overnight with agitation. For overexpression, anti-TOMM20 (Abcam, rabbit ab78547) and anti-Myc (Roche, mouse 11667149001) primary antibodies were used. For knockdown, anti-CHIP (Sigma, mouse S1073) was used instead of anti-Myc. The next day, cells were washed three times and incubated for 1 h at room temperature with agitation with secondary antibodies diluted in blocking buffer. Alexa Fluor conjugated secondary antibodies anti-mouse 555 (Life Technologies, a31570), and anti-rabbit 647 (Life Technologies, a21245) were utilized. Following the incubation, cells were washed twice followed by a 5 min incubation with 300 nM 4′,6-Diamidino-2-Phenylindole (DAPI) in PBS. Cover slips were mounted with DAKO fluorescence mounting media (Agilent Technologies, S3023). A Zeiss LSM880 confocal microscope was used to image slides at 20× magnification (Advanced Optical Microscopy Facility at Write Cell Imaging Facility). GFP-Parkin puncta colocalization with TOMM20 was scored by eye by an individual blinded to treatment conditions. A minimum of 150 cells were counted per condition.

2.5. Mito-mKeima mitophagy assay

Mito-mKeima mitophagy assay was performed as previously described (De Snoo et al., 2019). U2OS cells stably expressing GFP-Parkin and ecdysone inducible mitochondrially targeted mito-mKeima (mt-Keima), a pH-dependent fluorescence protein, were used. Cells

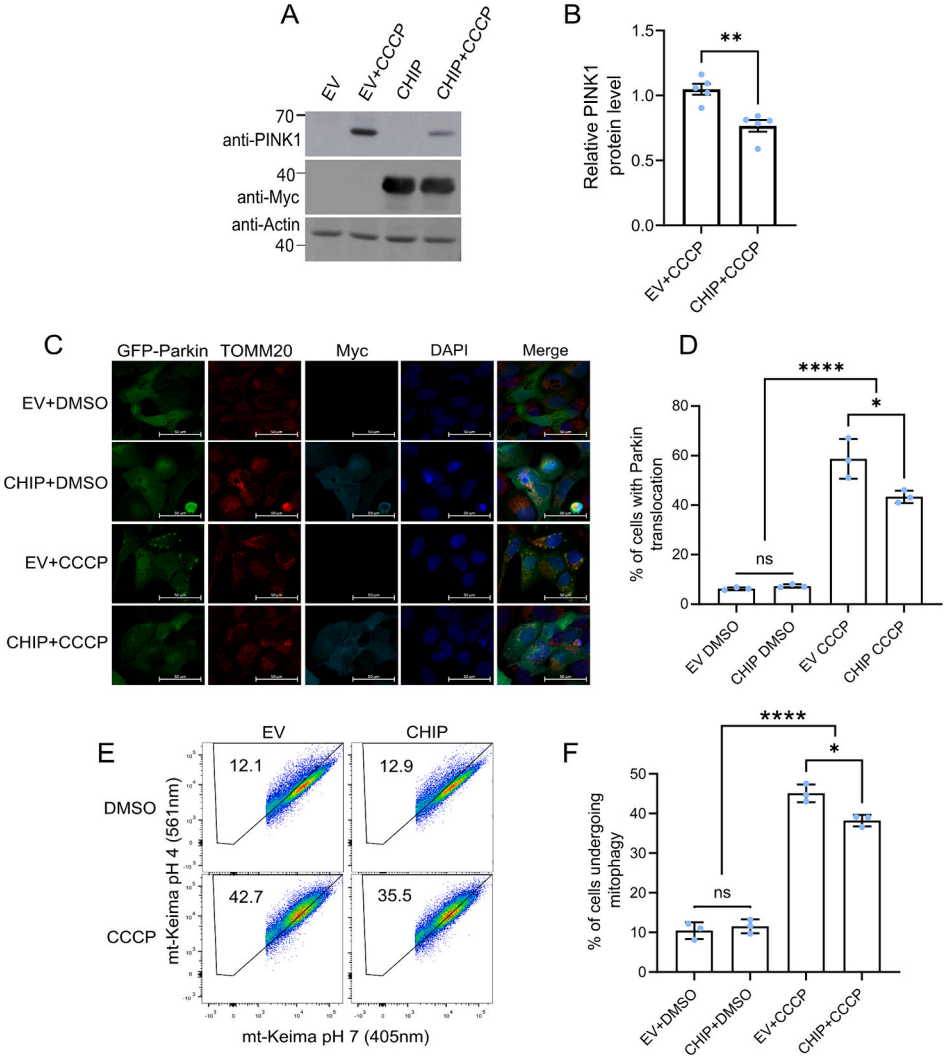

Fig. 1. CHIP overexpression reduces PINK1/Parkin-mediated mitophagy in response to CCCP treatment. A) Representative Western blot of PINK1 protein levels following CHIP overexpression and subsequent treatment with CCCP or DMSO. B) PINK1 protein levels in CCCP treated conditions were quantified with ImageJ and normalized to actin. Data is represented as mean ± SD of $N = 5$ independent experiments. Statistical analysis was performed using unpaired *t*-test. $^{**}p < 0.01$. C) Representative immunofluorescence of U2OS cells expressing GFP-Parkin, transfected with EV or Myc-CHIP, and subsequently treated with 20 μM CCCP or DMSO for 1 h prior to fixing and permeabilization. Cells were stained for the mitochondrial marker TOMM20, Myc, and the nuclear marker DAPI. Scale bar is 50 μm. D) Quantification of the percentage of cells with GFP puncta colocalized with TOMM20 was scored by eye and the scorer was blinded to treatment conditions. Bars represent mean ± SD of $N = 3$ independent experiments. Statistical analysis was performed using One-way ANOVA with Tukey's *post hoc* test. $^{**}p < 0.01$, $^{****}p < 0.0001$. E) Representative flow cytometry dot plots of U2OS cells stably expressing GFP-Parkin and mt-Keima. Cells were transfected with EV or Myc-CHIP, treated with 20 μM CCCP or DMSO for 4 h, and subsequently assessed by flow cytometry. X-axis is a measure of mt-Keima pH 7 (405 nm) and y-axis is a measure of mt-Keima pH 4 (561 nm). Cells within the upper gate were quantified as undergoing mitophagy. F) Quantification of the average percentage of cells undergoing mitophagy. Data is represented as mean ± SD of $N = 3$ independent experiments. Each condition was performed in technical triplicate and the averaged value was used for each independent experiment. Statistical analysis was performed using One-way ANOVA with Tukey's *post hoc* test. $^{**}p < 0.01$, $^{****}p < 0.0001$. CCCP: carbonyl cyanide *m*-chlorophenylhydrazone; CHIP: C-terminus of HSP70 interacting protein; DAPI: 4′,6-diamidino-2-phenylindole; DMSO: dimethyl sulfoxide; EV: empty vector; GFP: green fluorescent protein; mt-Keima: mito-mKeima; PINK1: PTEN-induced kinase 1; TOMM20; translocase of the outer mitochondrial membrane 20. (For interpretation of the references to colour in this figure legend, the reader is referred to the web version of this article.)

were transfected as described previously. 24 h post plasmid transfections and 48 h post siRNA transfection, cells were treated with 10 μM Ponasterone A (BioShop, PON123.5) for 24 h to induce mito-mKeima expression. Cells were then treated with 20 μM CCCP or DMSO for 4 h. Cells were subsequently harvested using 0.05% trypsin-EDTA (ThermoFisher, 25200054), washed with PBS and analyzed using the LSR Fortessa Cell Analyzer (BD Bioscience) (Figs. 1 and 2) or the CytoFLEX LX flow cytometer (Beckman Coulter) (Fig. 4) at the Princess Margret Flow Cytometry Facility with 405 and 561 nm lasers and 610/20 filters. For each sample, 50,000 events were collected, and cells were gated for GFP-Parkin and mt-Keima expression. Mitophagy was assessed as the percentage of cells displaying an elevated 561/405 nm ratio as captured in the upper gate. This upper gate was defined by a control sample reflecting the baseline mitophagy seen in our system (3–5%), as we have previously described (Tang et al., 2017; De Snoo et al., 2019; McLelland et al., 2018). Data was analyzed using FlowJo VX software as described previously (Tang et al., 2017).

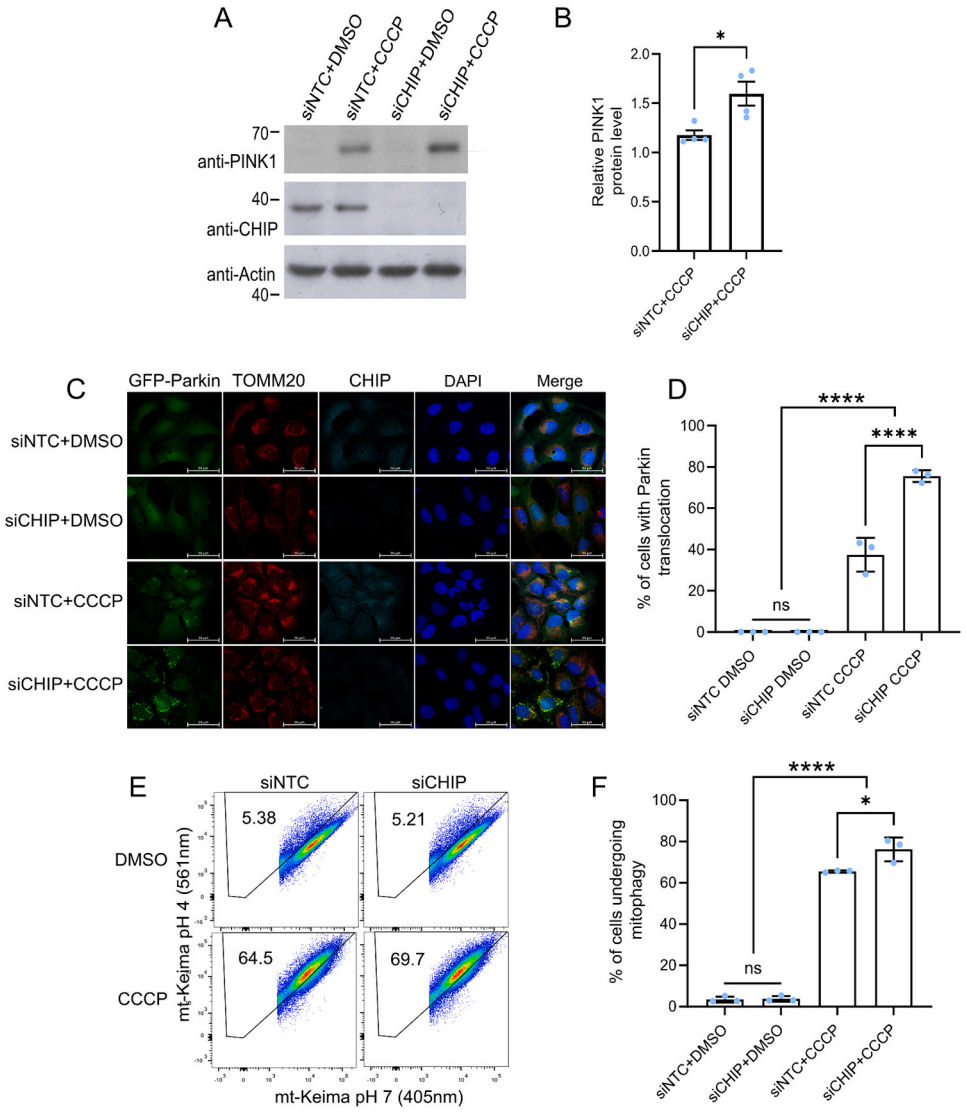

Fig. 2. CHIP knockdown increases PINK1/Parkin-mediated mitophagy in response to CCCP treatment. A) Representative Western blot of PINK1 protein levels in U2OS GFP-Parkin cells following CHIP knockdown and treatment with CCCP or DMSO. B) PINK1 levels in CCCP treated conditions were quantified using ImageJ analysis and normalized to actin. Data is represented as mean ± SD of $N = 4$ independent experiments. Statistical analysis was performed using unpaired *t*-test. *$p < 0.05$. C) Representative immunofluorescence of U2OS cells expressing GFP-Parkin transfected with siNTC or siCHIP and treated with 10 μM CCCP or DMSO for 1 h prior to fixing. Cells were permeabilized and stained for the mitochondrial marker TOMM20, CHIP, and the nuclear marker DAPI. Scale bar is 50 μm. D) Quantification of the percentage of cells with GFP puncta colocalized with TOMM20 was scored by eye while the scorer was blinded to treatment conditions. Bars represent mean ± SD of $N = 3$ independent experiments. Statistics performed using One-way ANOVA with Tukey's *post hoc* test. ****$p < 0.0001$. E) Representative flow cytometry dot plots of U2OS cells stably expressing GFP-Parkin and mt-Keima. Cells were transfected with siNTC or siCHIP, treated with 20 μM CCCP or DMSO for 4 h, and subsequently assessed by flow cytometry. X-axis is a measure of mt-Keima pH 7 (405 nm) and y-axis is a measure of mt-Keima pH 4 (561 nm). Cells within the upper gate were quantified as undergoing mitophagy. F) Quantification of the percentage of cells undergoing mitophagy. Data is represented as mean ± SD of N = 3 independent experiments. Each condition was performed in technical triplicate and the averaged value was used for each individual experiment. Statistical analysis was performed with One-way ANOVA with Tukey's *post hoc* test. *$p < 0.05$, ****p < 0.0001. CCCP: carbonyl cyanide *m*-chlorophenylhydrazone; CHIP: C-terminus of HSP70 interacting protein; DAPI: 4′,6-diamidino-2-phenylindole; DMSO: dimethyl sulfoxide; GFP: green fluorescent protein; HMW: high molecular weight; mt-keima: mito-keima; PINK1: PTEN-induced kinase 1; siCHIP: siRNA targeting CHIP; siNTC: non-targeting siRNA; TOMM20; translocase of the outer mitochondrial membrane 20. (For interpretation of the references to colour in this figure legend, the reader is referred to the web version of this article.)

2.6. Western blot

Western blots were performed as previously described (Friesen et al., 2020). Cells were collected with ice cold PBS and lysed using RIPA (50 mM Tris-HCl pH 7.4, 2 mM EDTA pH 8.0, 150 mM NaCl, 1% TritonX-100) with cOmplete protease inhibitor (Sigma, 11836153001). Whole cell lysates were prepared with 6× Laemmli sample buffer (375 mM Tris HCl, 9% SDS, 50% glycerol, 0.03% Bromophenol blue), boiled at 95 °C for 10 min, and run on 10% SDS PAGE gels. Gels were transferred onto a polyvinylidene fluoride (Bio-Rad, 1620177) membrane. Membranes were blocked with 5% *w/v* milk in tris-buffered saline (TBS) with 0.1% Tween20 (TBS-T) and probed with primary antibodies for 1 h at room temperature or overnight at 4 °C. Membranes were washed three times for 5 min at room temperature with TBS-T and then probed with secondary antibodies for 1 h at room temperature. Blots were washed three times with TBS-T and visualized.

Antibodies used include anti-Flag M2 (Sigma, F3165), anti-Flag (Sigma, F4725), anti-Actin (Sigma, A2066), anti-GFP (Life-Technologies, A11120) anti-Myc (Roche, 11667149001), anti-Ub (Santa Cruz, sc-8017), anti-GST HRP (GE Healthcare, RPN1236V), anti-PINK1 (Cell Signaling, 6946 s), anti-TOMM20 (Abcam, ab78547) and anti-CHIP (Sigma, S1073).

Secondary antibodies used were: sheep anti-mouse HRP (GE Healthcare, NA931), donkey anti-rabbit HRP (GE Healthcare, NA934), donkey anti-rabbit IRDye 680RD (Li-Cor, 926–68073), and goat anti-mouse IRDye 800CW (Li-Cor, 926–32210). For HRP-linked secondary antibodies, signal was detected using Pierce ECL Western Blotting Substrate (ThermoScientific, 32209) and developed on HyBlot CL autoradiography film (Denville Scientific, E3018). IRDye secondary antibodies were visualized with the Odyssey Infrared Imaging System (Li-Cor, 9120).

2.7. Immunoprecipitation

Immunoprecipitations were performed as previously described (De Snoo et al., 2019; Friesen et al., 2020). HEK293 cells were transfected, collected, and lysed as described for Western blot analysis. 300 μg of protein lysate was resuspended to 500 μl total volume with RIPA buffer and was incubated at 4 °C overnight on a head-over-head rotator with 1 μg of anti-Flag M2 (Sigma, F3165) antibody. Subsequently, 50 μl of Protein G Sepharose 4 Fast Flow (Cytiva, 17061801) was washed, resuspended in RIPA, added to IPs, and incubated at 4 °C for 4 h on a head-over-head rotator. IPs were centrifuged at 2000*g* for 5 min at 4 °C, supernatant was removed, and 1 ml RIPA was added to resuspend beads. Beads were washed 4 times. The final supernatant was removed and beads were resuspended in Laemmli loading dye, boiled at 95 °C for 10 min, and subsequently assessed by Western Blot. Ten% of the amount of protein used for each IP was loaded to Western blots as inputs.

2.8. Recombinant proteins

pDEST565-CHIP constructs were generated as previously described and transformed into BL21(DE3) competent cells (NEB, C2527I) according to manufacturer's protocol. Protocol for the production of recombinant CHIP protein was modified from a protocol provided to us by Dr. Matthew Scaglione (Umano et al., 2022). BL21(DE3) cells were grown in lysogeny broth (LB) at 37 °C with shaking until OD600 = ~0.8. Cells were then cooled in ice water, induced with 0.1 mM IPTG (BioShop, IPT001) and grown at 15 °C for 20 h. Cells were pelleted for 10 min at 2000 g, resuspended in modified NETN buffer (100 mM NaCl, 20 mM Tris-Cl pH 8.0, 0.5% *v*/v NP-40) with 1 mM PMSF (BioShop, PMS123.5) and lysed by sonication 3× for 20 s. After sonication, samples were spun at 4 °C for 20 min at 20,000 g and the supernatant containing recombinant protein was collected. GST-CHIP was purified from the supernatant using glutathione Sepharose 4B (Cytiva, 17075601) according to manufacturer's protocol. Eluted recombinant protein was concentrated using a 50 kDa MWCO centrifugal filter concentrator (Amicon, UFC5050). Recombinant *in vitro* auto-ubiquitination was performed using the Human CHIP Ubiquitin Ligase Kit (R&D systems, K-280) according to manufacturer's protocol but the 10× HSP70/HSP40 Mix and 10× luciferase substrates were replaced with ddH2O.

For imaging recombinant proteins, SDS PAGE gels were washed once with ddH2O after running. Gels were then incubated for 1 h at room temperature in SimplyBlue SafeStain (Invitrogen, LC6060) and then washed overnight with ddH2O. Gels were imaged using ChemiDoc gel imaging system (Bio-Rad, 12003153).

2.9. C. elegans maintenance

C. elegans were maintained on nematode growth medium (NGM) agar plates with the *Escherichia coli* OP50 strain used as worm food at room temperature using standard strain maintenance techniques (Brenner, 1974). The following worm strains were used: N2: wild-type Bristol isolate, chn-1(by155)I, chn-1(tm2692)I, pink-1(tm1779)II, pdr-1(gk488)III, IR1864: N2; *Ex001*[$p_{unc\text{-}119}$TOMM-20::Rosella], IR2160: N2; *Ex002*[$p_{rab\text{-}3}$DsRed::LGG-1;$p_{rab\text{-}3}$DCT-1::GFP; $p_{myo\text{-}2}$GFP], PHX5417: *chn-1(syb5417)I* and PHX5418: *chn-1(syb5418)I*.

CRISPR-Cas9 mutant *C. elegans, chn-1(syb5417)* and *chn-1(syb5418)*, were generated by SunyBiotech (SunyBiotech, n.d.). The N2 strain is used as the canonical wild-type strain (Caenorhabditis Genetics Center (CGC), n.d.). Reporter expressing mutant lines as well as double mutant lines were generated by crossing males with hermaphrodites using standard techniques (Brenner, 1974). Worm lines utilized in this study are summarized in Table 1.

2.10. C. elegans mitophagy

Mitophagy assessment was performed as described previously (Palikaras and Tavernarakis, 2017). One day old adult hermaphrodite worms were utilized for mitophagy assessment. Worms were picked to 2% agarose pads with 20 mM levamisole (Santa Cruz, sc-205730 A) in M9 buffer (3 g/l KH_2PO_4, 6 g/l Na_2HPO_4, 5 g/l NaCl) and imaged using a Zeiss LSM880 confocal microscope. For the *C. elegans* line IR2160: N2; *Ex002*[$p_{rab\text{-}3}$DsRed::LGG-1;$p_{rab\text{-}3}$DCT-1::GFP; $p_{myo\text{-}2}$GFP], *Z*-stack images taken at 63× magnification were captured of the tails of IR2160 expressing worms. Imaris (Oxford instruments) coloc tool was used to quantify GFP co-localized with DsRed in the worm tail Z-stacks. IR1864: N2; *Ex001*[$p_{unc\text{-}119}$TOMM-20::Rosella] reporter expressing worms were imaged at 20× magnification. ImageJ was used to measure GFP and DsRed pixel intensity in the heads of mtRosella expressing worms.

Table 1
C. elegans lines used for this study.

Genotype	Reporter
WT N2	IR2160
chn-1(by155)	IR2160
WT N2	IR1864
chn-1(by155)	IR1864
chn-1(tm2692)	IR1864
chn-1(syb5147)	IR1864
chn-1(syb5148)	IR1864
pink-1(tm1779)	IR1864
pdr-1(gk488)	IR1864
chn-1(by155);pink-1(tm1779)	IR1864
chn-1(by155);pdr-1(gk488)	IR1864

The WT N2 strain was used as the canonical WT strain. The IR1864: N2; *Ex001*[$p_{unc\text{-}119}$TOMM-20::Rosella] and IR2160: N2; *Ex002*[$p_{rab\text{-}3}$DsRed::LGG-1;$p_{rab\text{-}3}$DCT-1::GFP; $p_{myo\text{-}2}$GFP] worm lines express pan-neuronal mitophagy reporters. chn-1: C-terminus of hsp70 interacting protein; pdr-1: Parkinson's disease related-1/Parkin; pink-1: PTEN-induced kinase 1; WT: wild-type.

2.11. Statistical analysis

All statistical analysis was performed using GraphPad Prism 9. ROUT analysis was used to identify outliers.

3. Results

3.1. CHIP overexpression reduces PINK1/Parkin-mediated mitophagy

As CHIP has been demonstrated to be a regulator of Parkin activity (Imai et al., 2002), and mitochondrial dynamics (Palubinsky et al., 2015), we first sought to determine if CHIP is a regulator of PINK1/Parkin-mediated mitophagy *in vitro*. To investigate the impact of CHIP overexpression on PINK1/Parkin-mediated mitophagy, *in vitro* experiments were performed in U2OS cells stably expressing GFP-Parkin. U2OS cells are specifically reliant on the PINK1/Parkin pathway for mitophagy (Tang et al., 2017; De Snoo et al., 2019), but do not express detectable levels of endogenous Parkin protein, and thus require the addition of Parkin for mitophagy induction (Tang et al., 2017; Durcan et al., 2014).

To examine the effects of CHIP overexpression on PINK1 protein levels, cells were transfected with a Myc-CHIP plasmid or empty vector control. Transfected cells were treated with the mitochondrial depolarizing compound carbonyl cyanide *m*-chlorophenyl hydrazone (CCCP) or dimethyl sulfoxide (DMSO) vehicle control and lysates were analyzed by Western blot (Fig. 1A). PINK1 protein was detectable by Western blot in CCCP treated cells, but not in DMSO treated cells. In CCCP treated cells, CHIP overexpression decreased PINK1 protein levels compared to empty vector control (Fig. 1B).

In order to understand if changes in CHIP impacted mitophagy, we next assessed the effects of CHIP overexpression on Parkin recruitment to mitochondria, an early step in the PINK1/Parkin mitophagy pathway. U2OS GFP-Parkin cells were transfected with Myc-CHIP or empty vector control and subsequently treated with CCCP or DMSO control prior to being fixed and stained. Parkin recruitment to the mitochondria was quantified by examining the colocalization of GFP-Parkin puncta with the OMM protein translocase of the outer mitochondrial membrane 20 (TOMM20) (Fig. 1C). CHIP overexpression reduced the percentage of cells with Parkin recruitment to the mitochondria in response to CCCP treatment compared to empty vector control (Fig. 1D), indicating an impairment in early mitophagy in CHIP overexpressing cells.

Given that CHIP negatively regulates PINK1 levels and Parkin translocation to mitochondria, we next examined the effects of CHIP on subsequent mitochondrial turnover by utilizing the mito-mKeima (mt-Keima) reporter (Tang et al., 2017; De Snoo et al., 2019; Durcan et al., 2014; Sun et al., 2017; Yi et al., 2019). Mt-Keima is a mitochondrial targeted pH-sensitive fluorescent protein which undergoes a shift in fluorescence excitation spectra when exposed to the acidic lysosomal lumen (Katayama et al., 2011), allowing for the measurement of lysosomal engulfment of mitochondria. U2OS GFP-Parkin cells stably expressing mt-Keima were transfected with Myc-CHIP or empty vector and subsequently treated with CCCP or DMSO control prior to being collected and analyzed by flow cytometry (Fig. 1E). In line with our Parkin recruitment findings, CHIP overexpression decreased the percentage of cells undergoing mitophagy in response to CCCP treatment compared to empty vector control treated cells (Fig. 1F). Overall, our results demonstrate that CHIP overexpression leads to a reduction in PINK1/Parkin-mediated mitophagy.

3.2. CHIP knockdown increases PINK1/Parkin-mediated mitophagy

To exclude the possibility that the observed effects of CHIP on mitophagy are exaggerated due to overexpression of exogenous CHIP, we tested if knockdown of endogenous CHIP enhances PINK1/Parkin-mediated mitophagy. U2OS GFP-Parkin cells were transfected with short interfering RNA (siRNA) targeting CHIP (siCHIP) or with a non-targeting control siRNA (siNTC), treated with CCCP or DMSO control, and analyzed by Western blot (Fig. 2A). As above, PINK1 was not detectable by Western blot in DMSO treated conditions. Following treatment with CCCP, CHIP knockdown increased PINK1 protein levels compared to siNTC control (Fig. 2B).

Next, we evaluated the effects of CHIP knockdown on Parkin recruitment to the mitochondria. U2OS GFP-Parkin cells were transfected with siCHIP or siNTC and treated with CCCP or DMSO control prior to being fixed and stained (Fig. 2C). Knockdown of CHIP increased the percentage of cells with Parkin puncta localized to mitochondria compared to siNTC control treated cells in response to CCCP treatment (Fig. 2D).

Lastly, we assessed the impact of CHIP knockdown on mitophagy. U2OS GFP-Parkin cells expressing mt-Keima were transfected with siNTC or siCHIP and treated with CCCP or DMSO control prior to being collected and analyzed by flow cytometry (Fig. 2E). CHIP knockdown significantly increased the percentage of cells undergoing mitophagy in response to CCCP treatment compared to siNTC transfected control cells (Fig. 2F). These findings demonstrate that CHIP acts as a negative regulator of Parkin recruitment to mitochondria and PINK1/Parkin-mediated mitophagy.

3.3. Loss of CHIP increases neuronal mitophagy in C. elegans in a PINK1/Parkin-dependent manner

As we have demonstrated that CHIP is a negative regulator of PINK1/Parkin-mediated mitochondrial turnover and that its knockdown enhances mitophagy, we next sought to determine the impact of the loss of CHIP on mitophagy in neurons utilizing *Caenorhabditis elegans* as a model organism. To evaluate the effects of loss of CHIP on mitophagy in neurons, transgenic *C. elegans* lines expressing neuronal-specific reporters, IR2160 and IR1864 (Tang et al., 2017; Palikaras and Tavernarakis, 2017), were utilized. Reporter-expressing *chn-1(by155)* worms, which possess a loss of function mutation within the gene encoding CHN-1, the *C. elegans* homologue of CHIP, were generated by crossing *chn-1(by155)* worms with reporter-expressing worms.

First, the localization of phagosomes to mitochondria was assessed utilizing the IR2160 reporter worm line. The IR2160: N2; *Ex002*[$p_{rab\text{-}3}$DsRed::LGG-1;$p_{rab\text{-}3}$DCT-1::GFP; $p_{myo\text{-}2}$GFP] reporter worm line expresses a DsRed tagged LGG-1 (a *C. elegans* homologue of LC3) as well as a GFP tagged DCT-1 (an OMM protein). Using this reporter, phagosome recruitment to the mitochondria is quantified by the colocalization of the phagosome marker DsRed-LGG-1 with the mitochondrial marker GFP-DCT-1. IR2160 reporter-expressing wild-type (WT) and *chn-1 (by155)* worms were picked to agarose pads with anaesthesia and imaged by confocal fluorescence microscopy (Fig. 3A). *chn-1(by155)* worms displayed a significant increase in GFP colocalized to DsRed compared to WT control worms, indicating an elevation in the colocalization of mitochondria with phagosomes in the neurons of animals with loss of CHIP (Fig. 3B).

As phagosome recruitment to mitochondria was elevated in *chn-1 (by155)* worms compared to control, we next utilized the IR1864 reporter worm line to determine whether mitophagy is also elevated in worms with loss of CHIP function. The IR1864: N2; *Ex001*[$p_{unc\text{-}119}$TOMM-20::Rosella] worm expresses mtRosella, a protein comprised of a pH-stable DsRed fused to a pH-sensitive GFP, fused to the OMM localized protein TOMM-20. Under neutral pH conditions, mtRosella displays both GFP and DsRed fluorescence but, following the engulfment of mitochondria within the acidic lysosomal lumen, GFP signal is quenched while DsRed fluorescence is retained. Using this reporter, a decrease in GFP/DsRed intensity ratio indicates increased levels of lysosomal engulfment of mitochondria. IR1864 reporter-expressing worms were picked to agarose pads with anaesthesia, imaged using confocal fluorescence microscopy, and GFP and DsRed intensity was measured in worm heads (Fig. 3C). *chn-1(by155)* worms displayed a significant decrease in GFP/DsRed intensity ratio compared to WT

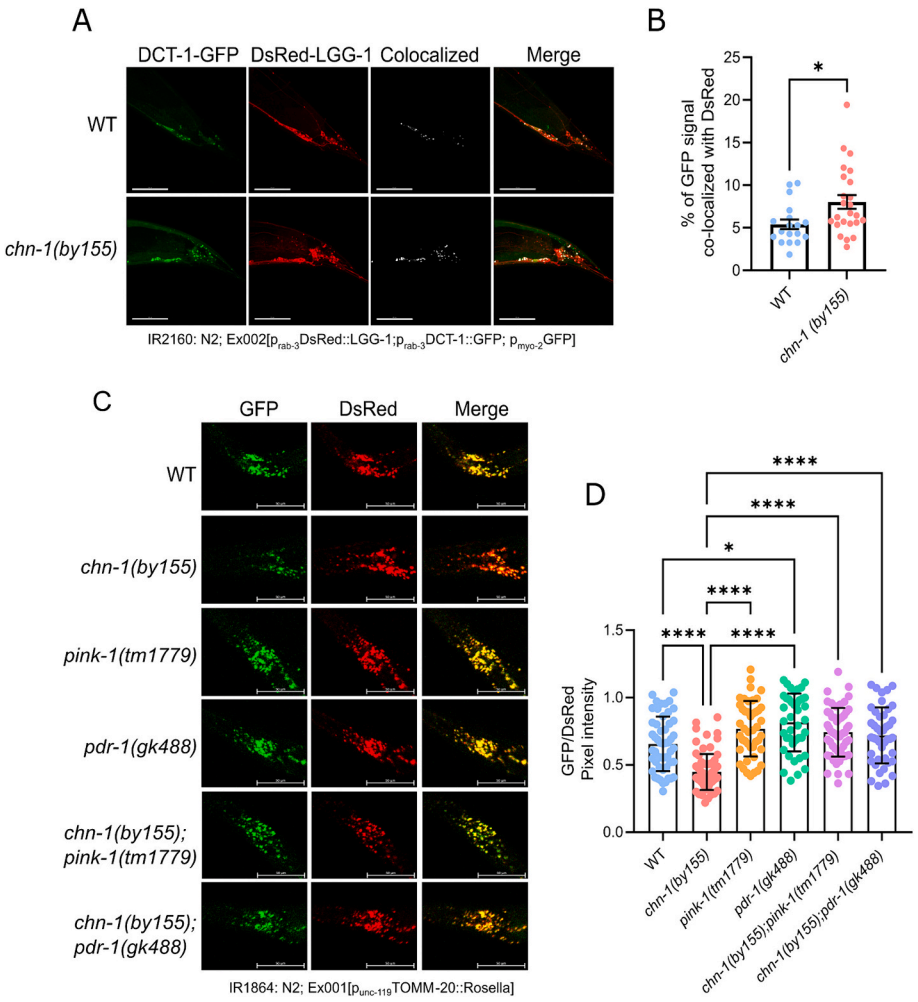

Fig. 3. Loss of the *C. elegans* homologue of CHIP, CHN-1, increases neuronal mitophagy *in vivo* in a PINK1 and Parkin dependent manner. A) The IR2160: N2; *Ex002* [$p_{rab\text{-}3}$DsRed::LGG-1;$p_{rab\text{-}3}$DCT-1::GFP; $p_{myo\text{-}2}$GFP] worm line which expresses DsRed-LGG-1 (a phagophore marker) and GFP-DCT-1 (a mitochondrial marker) was crossed into *chn-1(by155)* worms. Adult day 1 worms were picked to agar pads with anaesthesia and confocal fluorescence microscopy was utilized to take *Z*-stack images at 63× magnification. Maximum intensity projections and colocalization images of WT and *chn-1(by155)* worm tails were generated using Imaris software. Scale bar is 40 μm B) Quantification of the percentage of GFP signal colocalized with DsRed in tail Z-stacks was performed using the Imaris coloc tool. Bars represent mean ± SD of $N = 4$ independent experiments and individual points represent individual worms. Statistical analysis was performed using a Mann-Whitney test. *$p <$ 0.05. C) The IR1864: N2; *Ex001*[$p_{unc\text{-}119}$TOMM-20::Rosella] worm line with pan-neuronal expression of mtRosella, a mitochondrially targeted mitophagy reporter protein comprised of a pH-stable DsRed fused to a pH sensitive GFP, was crossed with various LOF mutant worm lines. Under normal physiological conditions, mitochondria are present under neutral pH conditions and mtRosella possesses both DsRed and GFP fluorescence. Within the acidic lysosomal lumen, GFP signal is quenched, resulting in only DsRed fluorescence. Adult day 1 worms were picked to agar pads with anaesthesia and imaged at 20× magnification using confocal fluorescence microscopy. GFP and DsRed pixel intensity were quantified in worm heads using ImageJ software and used to calculate GFP/DsRed pixel intensity ratio. Scale bar is 50 μm. D) Bars represent mean ± SD of N = 4 independent experiments. Each dot represents an individual worm. Statistical analysis was performed using Kruskal-Wallis test with Dunn's multiple comparisons test. *p < 0.05, ****$p <$ 0.0001. *chn-1*: C-terminus of HSP70 interacting protein; DCT-1: DAF-16/FOXO-controlled germline tumor affecting-1/mitochondrial marker; GFP: green fluorescent protein; LC3: microtubule-associated protein 1 light chain 3; LGG-1: *C. elegans* LC3 homologue/phagophore marker; LOF: loss of function; *pdr-1*: Parkinson's disease related 1/Parkin; pink-1: PTEN-induced kinase 1; TOMM-20: translocase of the outer mitochondrial membrane 20; WT; wild-type. (For interpretation of the references to colour in this figure legend, the reader is referred to the web version of this article.)

worms, indicating that mitophagy is elevated in worms with loss of CHIP compared to WT controls (Fig. 3D). Taken together, our findings indicate that neuronal mitochondria co-localize with phagosomes and undergo mitophagy at enhanced rates in worms with loss of CHIP.

To determine whether the increase in neuronal mitophagy observed in worms with loss of CHIP is dependent on PINK1 and Parkin, the IR1864 reporter was crossed into *pink-1(tm1779)* and *pdr-1(gk488)* worms, which possess null allele deletion mutations in the genes encoding the *C. elegans* homologues of PINK1 and Parkin, respectively. Reporter-expressing double mutant worm lines *chn-1(by155);pink-1 (tm1779)* and *chn-1(by155);pdr-1(gk488)* were also generated by crossing. *pdr-1(gk488)* worms exhibited a significantly increased GFP/DsRed intensity ratio compared to WT worms, indicating that loss of Parkin results in a reduction in neuronal mitophagy (Fig. 3D). *pink-1 (tm1779)* worms also displayed an increased GFP/DsRed intensity ratio compared to WT worms. Additionally, double mutant *chn-1(by155); pink-1(tm1779)* and *chn-1(by155);pdr-1(gk488)* worms displayed a significantly increased GFP/DsRed intensity ratio compared to *chn-1 (by155)* worms, indicating that neuronal mitophagy is reduced in double mutant worms compared to *chn-1(by155)* worms (Fig. 3D). This finding indicates that the increase in neuronal mitophagy observed in *chn-1(by155)* worms is dependent on both PINK1 and Parkin.

3.4. Disease-associated mutations in CHIP impair function including mitophagy regulation in vitro

As many disease-associated CHIP mutations have been demonstrated to reduce CHIP function, namely E3 ubiquitin ligase activity and/or cochaperone function (Pakdaman et al., 2021; Umano et al., 2022; Kanack et al., 2018; Madrigal et al., 2019), we hypothesized that disease-associated mutations will also have an impaired ability to negatively regulate mitophagy.

For this study, two patient-identified disease-associated CHIP mutations were selected for assessment: the TPR missense mutation I53T (Chen et al., 2020) and the Ubox frameshift mutation L275Dfs*16 (Genis et al., 2018; Lieto et al., 2020; Palvadeau et al., 2020; Magri et al., 2022; Barbier et al., 2022) (Table 2, Fig. 4A). Both the I53T and L275Dfs*16 mutations display an autosomal dominant pattern of inheritance and are associated with a high prevalence of ataxia and cognitive impairment. For both I53T and L275Dfs*16, cerebellar atrophy has been observed in all tested patients. The L275Dfs*16 mutation is the most frequently reported disease-associated CHIP mutation in patients and has currently been identified in 5 unrelated kindreds of different ethnic backgrounds.

Since CHIP is an E3 ubiquitin ligase, we first assessed the effects of the disease-associated mutations on E3 function. To assess E3 ubiquitin ligase function, GST-tagged recombinant WT and mutant CHIP proteins were generated and an *in vitro* auto-ubiquitination assay was performed. The L275Dfs*16 frameshift mutation, which results in a deletion of a portion of the Ubox domain, was unable to ubiquitinate itself, indicating an impairment in E3 ubiquitin ligase function (Fig. 4B). Conversely, the I53T CHIP mutant maintained the ability to auto-ubiquitinate.

Next, as CHIP is an HSP70 cochaperone, we assessed the ability of disease-associated CHIP mutants to interact with HSP70. HEK293 cells were co-transfected with GFP-HSP70 and FLAG-CHIP expression constructs or empty vector control. Subsequently, immunoprecipitation of CHIP was performed utilizing an anti-FLAG antibody (Fig. 4C). Mutations in CHIP did not result in changes in CHIP protein levels (Fig. 4D). Similarly to other mutations within the TPR domain (Kanack et al., 2018), the I53T CHIP mutant displayed a significant reduction in HSP70 interaction compared to WT CHIP (Fig. 4E). Conversely, the L275Dfs*16 mutation maintained the ability to interact with HSP70.

We next assessed the effects of disease-associated CHIP mutations on PINK1 protein levels and mitophagy. U2OS GFP-Parkin cells were transfected with FLAG-CHIP expression constructs or empty vector control prior to being treated with either CCCP or DMSO. PINK1 protein levels were assessed by Western blot (Fig. 4F). Unlike WT CHIP, disease-associated CHIP mutants were not associated with a reduction in PINK1 protein levels following CCCP treatment compared to empty vector control (Fig. 4G).

To assess mitophagy, U2OS GFP-Parkin cells stably expressing mt-Keima were transfected with FLAG-CHIP expression constructs or empty vector control, treated with CCCP, and collected and analyzed by flow cytometry as described above (Fig. 4H). Overexpression of WT CHIP significantly decreased the percentage of cells undergoing mitophagy in response to CCCP treatment compared to empty vector control treated with CCCP (Fig. 4I). Interestingly, the expression of either I53T or L275Dfs*16 CHIP mutants was not sufficient to decrease the percentage of cells undergoing mitophagy in response to CCCP treatment compared to empty vector control (Fig. 4I).

3.5. Both I53T and L275Dfs*16 disease-analogous mutations elevate neuronal mitophagy in C. elegans

To determine whether I53T or L275Dfs*16 disease-associated CHIP mutations have an altered ability to regulate mitophagy *in vivo*, CRISPR-Cas9 was utilized to generate *C. elegans* lines with endogenous disease-analogous mutations within the *chn-1* gene. The analogous mutations for I53T and L275Dfs*16 in human CHIP are I32T and L233Yfs*2 in CHN-1 respectively (Table 3, Fig. 5A). CHN-1 I32T *(chn-1(syb5417))* and CHN-1 L233Yfs*2 *(chn-1(syb5418))* CRISPR mutant worm lines were generated and utilized for experiments as homozygous mutants.

To assess how these disease-analogous mutations affect neuronal mitophagy in *C. elegans*, CHN-1 I32T and CHN-1 L233Yfs*2 mutant worms were crossed with the IR1864 mtRosella mitophagy reporter line and reporter-expressing worms were imaged utilizing confocal fluorescence microscopy (Fig. 5B). Reporter-expressing WT and *chn-1* loss of function deletion worm lines, *chn-1(by155)* and *chn-1(tm2692)*, were utilized as controls. All *chn-1* mutant worm lines, including the disease-analogous CRISPR mutant worms, displayed a significant increase in neuronal mitophagy compared to WT control worms (Fig. 5C). Despite its analogous human mutation maintaining the ability to regulate mitophagy *in vitro* in response to stress, the I32T mutation in *C. elegans* did result in an increase in neuronal mitophagy. These findings indicate that, in *C. elegans*, disease-analogous mutations in either the TPR or the Ubox domain can increase neuronal mitophagy compared to WT worms.

4. Discussion

In the present study, we demonstrate that *in vitro* overexpression of CHIP decreased PINK1 protein levels, suppressed Parkin recruitment to mitochondria and reduced mitophagy in response to CCCP treatment. Furthermore, knockdown of endogenous CHIP increased PINK1 protein levels, Parkin localization to mitochondria and mitophagy in response to CCCP treatment. Taken together, we identify CHIP acts as a negative regulator of PINK1/Parkin-mediated mitophagy *in vitro*. Consistent with our *in vitro* findings, we found that worms with loss of CHIP displayed elevated levels of neuronal mitophagy *in vivo* and this increase was dependent on both PINK1 and Parkin. Additionally, we demonstrate that the disease associated CHIP mutation I53T has impaired HSP70 interaction, and the L275Dfs*16 mutation has impaired E3 ubiquitin ligase function. Interestingly, overexpression of either the I53T or L275Dfs*16 mutant were not sufficient to reduce PINK1 protein levels or mitophagy in response to CCCP treatment *in vitro*. Additionally, *C. elegans* possessing endogenous CRISPR mutations analogous to either I53T or L275Dfs*16 displayed elevated neuronal mitophagy. Overall, we demonstrate that CHIP has a role in negatively regulating mitophagy and disease-associated mutations in CHIP may result in dysregulation of this pathway.

As CHIP negatively regulated PINK1 protein levels, a key initiator of PINK1/Parkin-mediated mitophagy, we propose that CHIP negatively regulates mitophagy by reducing PINK1 protein levels. Moreover, disease-associated CHIP mutants, which were unable to reduce PINK1 protein levels, failed to hinder mitophagy. A previous study demonstrated that CHIP ubiquitinates PINK1 in an HSP70-dependent manner, promoting its proteasomal degradation in HEK293 cells and mouse embryonic fibroblasts (MEFs) (Yoo and Chung, 2018), which may explain how CHIP negatively regulates PINK1 protein levels in our

Table 2
SCA48-associated mutations utilized for *in vitro* analysis.

CHIP mutation (RefSeq NP_005852.2)	*STUB1* mutation (RefSeq NM_005861.4)	Type of Mutation	# of patients identified	# of kindreds identified
p.I53T	c.158 T > C	Missense	4	1
p.L275Dfs*16	c.823_824delCT	Frameshift deletion	13	5

Mutations in the CHIP protein and cDNA (*STUB1* mutation) chosen for this study are listed. CHIP: C-terminus of HSP70 interacting protein; del: deletion; fs: frameshift; SCA48: spinocerebellar ataxia autosomal dominant type 48; STUB1: STIP1 homology and Ubox containing protein 1.

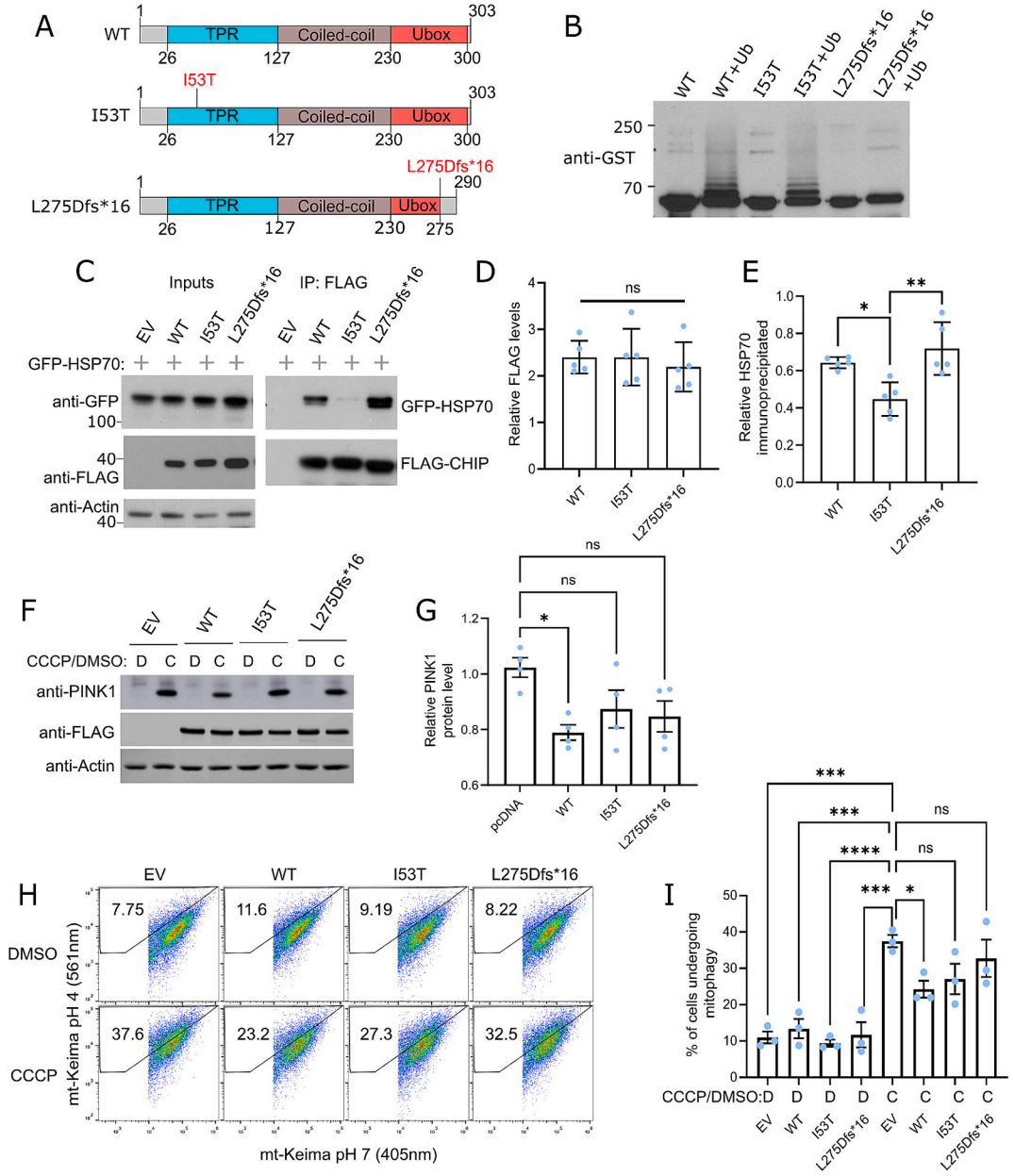

Fig. 4. Disease-associated mutants have impairments in function, including the ability to negatively regulate mitophagy. A) Schematic diagrams of WT, I53T and L275Dfs*16 CHIP proteins. The position of the selected variants is shown in red. Diagram was generated using DOG 2.0 software. B) Purified recombinant GST-CHIP proteins were utilized in an *in vitro* auto-ubiquitination assay and assessed by Western blot. Blot is representative of $N = 3$ independent experiments. C) HEK293 cells were co-transfected with GFP-HSP70 and FLAG-CHIP constructs. Inputs were 10% of total protein used for each IP. IP with anti-FLAG antibody was probed for GFP. D) Quantification of FLAG-CHIP proteins was quantified using ImageJ and normalized to actin. Bars represent mean ± SD of $N = 5$ experiments. Statistical analysis was performed using One-way ANOVA. E) Quantification of GFP-HSP70 levels immunoprecipitated by anti-FLAG immunoprecipitation. Bars represent mean ± SD of $N = 5$ individual experiments. Statistical analysis was performed using One-way ANOVA with Tukey's *post hoc* test. *$p < 0.05$, **$p < 0.01$. F) Representative Western blot of PINK1 protein levels in U2OS GFP-Parkin cells following overexpression of WT and mutant FLAG-CHIP proteins followed by treatment with CCCP or DMSO. G) PINK1 levels in CCCP treated conditions were quantified using ImageJ analysis and normalized to actin. Data is represented as mean ± SD of $N = 4$ independent experiments. Statistical analysis was performed using One-way ANOVA with Tukey's *post hoc* test. *$p < 0.05$. H) Representative flow cytometry dot plots from U2OS GFP-Parkin mt-Keima cells transfected with EV or FLAG-CHIP expression plasmids. Cells were treated with DMSO or 20 μM CCCP for 4 h and subsequently analyzed by flow cytometry. X-axis is a measure of mt-Keima pH 7 (405 nm) and y-axis is a measure of mt-Keima pH 4 (561 nm). Cells within the upper gate were quantified as undergoing mitophagy. I) Quantification of the percentage of cells undergoing mitophagy. Bars represent mean ± SD of $N = 3$ independent experiments. Each condition was performed in technical triplicate and mean value was used for each independent experiment. Statistical analysis was performed with One-way ANOVA with Dunnett's multiple comparisons test compared to EV + CCCP. *p < 0.05, ***$p < 0.001$, ****$p < 0.0001$. CCCP: carbonyl cyanide *m*-chlorophenylhydrazone; CHIP: c-terminus of HSP70 interacting protein; DMSO: dimethyl sulfoxide; EV: empty vector; fs: frameshift; GFP: green fluorescent protein; HSP70; heat shock protein 70; IP: immunoprecipitation; mt-Keima: mito-mKeima; SCA48: spinocerebellar ataxia autosomal dominant type 48; TPR; tetratricopeptide repeat region; WT: wild-type. (For interpretation of the references to colour in this figure legend, the reader is referred to the web version of this article.)

Table 3
Analogous disease-associated mutations in *C. elegans*.

CHIP mutation (RefSeq NP_005852.2)	*STUB1* mutation (RefSeq NM_005861.4)	Type of Mutation	CHN-1 mutation (RefSeq NP_491781.2)	*chn-1* mutation (RefSeq NM_059380.6)
p.I53T	c.158 T > C	Missense	p.I32T	c.105 T > C
p.L275Dfs*16	c.823_824delCT	Frameshift deletion	p.L233Yfs*2	c.697_698delCT

Disease-associated mutations in the CHIP protein and *STUB1* cDNA chosen for analysis are listed alongside their analogous mutations in the *C. elegans chn-1* protein and gene. cDNA: complementary DNA; CHIP: C-terminus of HSP70 interacting protein; CHN-1: C-terminus of HSP70 interacting protein (*C. elegans*); del: deletion; fs: frameshift; STUB1: STIP1 homology and Ubox containing protein 1.

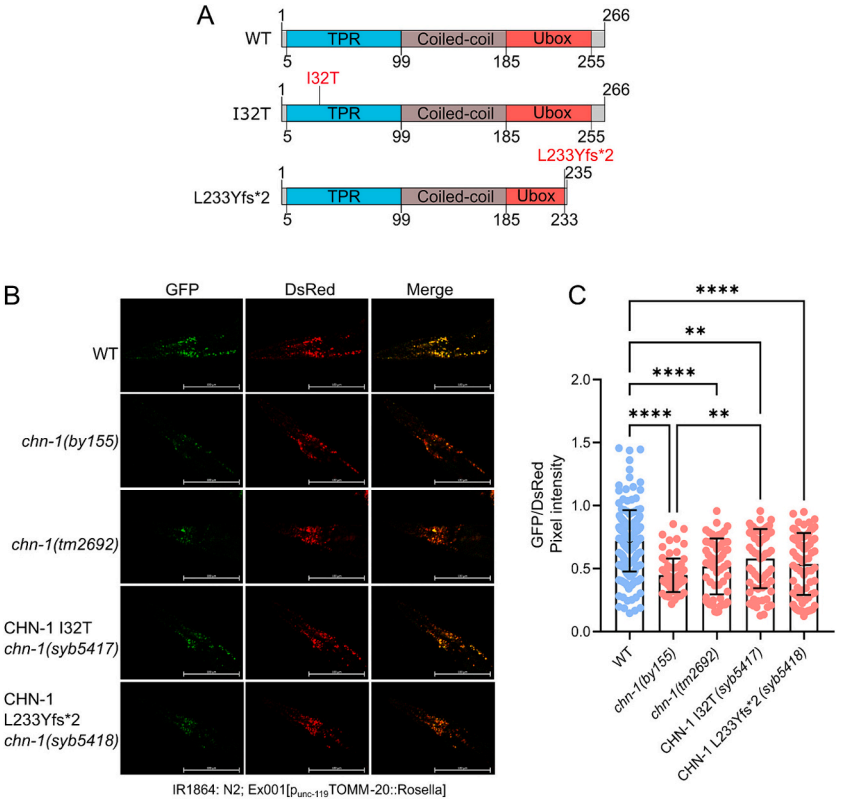

Fig. 5. Disease-associated mutations in *C. elegans* increase neuronal mitophagy *in vivo*. A) Schematic diagram of the analogous mutations to our SCA48-associated mutations of interest. I32T CHN-1 *(chn-1(syb5417))* encodes a missense mutation within the TPR domain which is analogous to the human CHIP I53T mutation. L233Yfs*2 CHN-1 *(chn-1(syb5418))* encodes a Ubox frameshift mutation which is analogous to the human L275Dfs*16 mutations and results in a truncation of the Ubox domain and shortening of the total protein. The position of the selected variants is shown in blue. Figure was generated using DOG 2.0 software. B) The IR1864: N2; *Ex001*[$p_{unc\text{-}119}$TOMM-20::Rosella] worm line, which expresses the mtRosella mitophagy reporter protein pan-neuronally, was crossed with *chn-1* mutant worm lines. MtRosella is comprised of a pH-stable DsRed fused to a pH sensitive GFP. Under physiological conditions, mitochondria are at a neutral pH and mtRosella possesses both DsRed and GFP fluorescence, but within the acidic lysosomal environment, GFP signal is quenched, resulting in only DsRed fluorescence. Adult day 1 worms were picked to agar pads with anaesthesia and live worms were imaged at 20× magnification using confocal fluorescence microscopy. Scale bar is 100 μm. C) GFP and DsRed pixel intensity were quantified within worm heads using ImageJ software. All *chn-1* mutant worms displayed a significantly decreased GFP/DsRed pixel intensity ratio compared to WT worms, indicating a significant increase in neuronal mitophagy. Bars represent mean ± SD of $N = 3$ independent experiments. Each dot represents an individual worm. Statistical analysis was performed using Kruskal-Wallis test with Dunn's multiple comparisons test. **p < 0.01, ****p < 0.0001. CHIP: c-terminus of HSP70 interacting protein (Human); CHN-1; c-terminus of HSP70 interacting protein (*C. elegans*); CRISPR: clustered regularly interspaced short palindromic repeats; fs: frameshift; GFP: green fluorescent protein; LOF: loss of function; SCA48: spinocerebellar ataxia autosomal dominant type 48; TOMM-20: translocase of the outer mitochondrial membrane 20; TPR: tetratricopeptide repeat region; WT: wild-type. (For interpretation of the references to colour in this figure legend, the reader is referred to the web version of this article.)

system. As both HSP70 interaction and E3 ubiquitin ligase function were required for CHIP to promote the proteasomal degradation of PINK1, this may explain why both tested disease-associated mutations displayed an impaired ability to reduce PINK1 protein levels and to negatively regulate mitophagy. Nevertheless, further investigation is required to dissect out the exact mechanism by which CHIP negatively regulates PINK1/Parkin-mediated mitophagy. It is also possible that CHIP may regulate PINK1/Parkin-mediated mitophagy through multiple mechanisms including by regulating macroautophagy. In MEFs, knockout of CHIP was demonstrated to reduce macroautophagy (Sha et al., 2017), while in HEK293 and N2a cells, knockdown of CHIP was observed to result in an increase in macroautophagy (Guo et al., 2015). Further investigation is required to understand how CHIP may regulate macroautophagy, and whether this plays a role in CHIP-mediated regulation of mitophagy.

Since disease-associated CHIP mutations resulted in dysregulation of mitophagy both *in vitro* and *in vivo* in *C. elegans* neurons, this may suggest that mitophagy dysregulation could be a component of CHIP-

associated diseases. It has been previously demonstrated that Purkinje neurons display high levels of basal mitophagy compared to other neuronal subtypes (McWilliams et al., 2016) and that elevated mitophagy was observed to precede neuron loss in a rat model of Purkinje neuron degeneration (Chakrabarti et al., 2009). These findings suggest that Purkinje neurons are vulnerable to mitophagy dysregulation, which could explain their specific susceptibility in CHIP-associated diseases.

While we found CHIP acted as a negative regulator of PINK1/Parkin-mediated mitophagy in both U2OS cells and *C. elegans* neurons, differences were observed in mitophagy activation between these systems. In *C. elegans*, loss of CHIP significantly elevated mitophagy in neurons, while in cells, treatment with a mitochondrial stressor was necessary to observe changes in mitophagy in response to altered CHIP expression. Why loss of CHIP increases neuronal mitophagy in worms without any additional stressors, but the addition of a mitophagy-inducing compound was necessary to observe an increase in mitophagy in U2OS GFP-Parkin cells following CHIP knockdown, is not clear. It is possible that, because siRNA-mediated knockdown does not entirely eliminate the target protein, the remaining CHIP protein impairs the initiation of mitophagy, and that the complete loss of CHIP is required to increase mitophagy without the addition of a mitophagy-inducing compound. Interestingly, in *C. elegans,* loss of function mutations in either PINK1 or Parkin significantly reduced basal neuronal mitophagy compared to WT control, while in U2OS GFP-Parkin cells we have preciously demonstrated that basal mitophagy is not significantly altered following the knockdown of PINK1 or in the absence of Parkin (De Snoo et al., 2019). As loss of PINK1 or Parkin significantly decreased basal mitophagy in worm neurons, this may indicate that some basal PINK1/Parkin-mediated mitophagy is occurring in *C. elegans* neurons, which does not appear to be the case in U2OS GFP-Parkin cells. Although PINK1/Parkin-mediated mitophagy has been overwhelmingly implicated in stress-induced, but not basal, mitophagy (McWilliams et al., 2018; Liu et al., n.d.; Lee et al., 2018), low levels of basal PINK1/Parkin-mediated mitophagy has been reported in certain cell types (Lee et al., 2018; Cornelissen et al., 2018). Taken together, it is possible that differences in relative levels of basal mitophagy may explain the differences observed between *C. elegans* neurons and U2OS cells in this study. Conversely, it may be the case that the mitophagy reporters utilized in *C. elegans* are more sensitive than the assays utilized in U2OS GFP-Parkin cells, allowing for changes in mitophagy in *C. elegans* neurons to be detected without the addition of a mitophagy-inducing stressor. Despite the differences observed between *C. elegans* neurons and U2OS cells in this study, CHIP acted as a negative regulator of mitophagy in both models.

Our study identifies CHIP as a negative regulator of mitophagy both *in vitro* and *in vivo*. Moreover, we show that disease-associated mutations in CHIP can result in dysregulation of mitophagy *in vivo*. Currently, there are no therapeutic strategies for the treatment of CHIP-associated diseases. Our results suggest that mitophagy regulation could be a valuable strategy for the development of novel disease-modifying treatments for CHIP-associated neurodegeneration.

Funding

RE and SH received support for the Mitochondrial Innovation Initiative (MITO2i). SKK and LVK are supported by CIHR.

CRediT authorship contribution statement

Rebecca Earnshaw: Writing – original draft, Visualization, Investigation, Formal analysis, Conceptualization. **Yu Tong Zhang:** Investigation. **Gregory Heymann:** Investigation. **Kazuko Fujisawa:** Writing – review & editing, Investigation. **Sarah Hui:** Investigation. **Minesh Kapadia:** Writing – review & editing. **Lorraine V. Kalia:** Supervision, Conceptualization. **Suneil K. Kalia:** Writing – review & editing, Supervision, Conceptualization.

Declaration of competing interest

The authors declare that they have no conflicts of interest with the contents of this article.

Data availability

Data will be made available on request.

Acknowledgements

LVK holds the Wolfond-Krembil Chair in Parkinson's Disease Research. SKK holds the R.R. Tasker Chair in Stereotactic and Functional Neurosurgery.

U2OS cells stably expressing GFP-Parkin or both GFP-Parkin and mito-mKeima were a gift from Dr. Edward Fon and Dr. Matthew Tang and were generated as previously described (Tang et al., 2017; Durcan et al., 2014). Protocol for the production of recombinant CHIP protein was modified from a protocol provided to us by Dr. Matthew Scaglione (Umano et al., 2022).

Appendix A. Supplementary data

Supplementary data to this article can be found online at https://doi.org/10.1016/j.nbd.2024.106625.

References

Ballinger, C.A., Connell, P., Wu, Y., Hu, Z., Thompson, L.J., Yin, L.Y., Patterson, C., 1999. Identification of CHIP, a novel tetratricopeptide repeat-containing protein that interacts with heat shock proteins and negatively regulates chaperone functions. Mol. Cell. Biol. 19, 4535–4545.

Barbier, M., Davoine, C.-S., Petit, E., Porché, M., Guillot-Noel, L., Sayah, S., Fauret, A.-L., Neau, J.-P., Guyant-Maréchal, L., Deffond, D., et al., 2022. Intermediate repeat expansions of TBP and STUB1: genetic modifier or pure digenic inheritance in spinocerebellar ataxias? Genet. Med. S1098-3600 (22), 00995–00999.

Bettencourt, C., de Yébenes, J.G., López-Sendón, J.L., Shomroni, O., Zhang, X., Qian, S.-B., Bakker, I.M.C., Heetveld, S., Ros, R., Quintáns, B., et al., 2015. Clinical and neuropathological features of spastic Ataxia in a Spanish family with novel compound heterozygous mutations in STUB1. Cerebellum 14, 378–381.

Brenner, S., 1974. The genetics of caenorhabditis elegans. Genetics 77, 71–94.

Caenorhabditis Genetics Center (CGC), 2024. College of Biological Sciences. https://cgc.umn.edu/.

Chakrabarti, L., Eng, J., Ivanov, N., Garden, G.A., La Spada, A.R., 2009. Autophagy activation and enhanced mitophagy characterize the Purkinje cells of pcd mice prior to neuronal death. Mol. Brain 2, 24.

Chen, D.-H., Latimer, C., Yagi, M., Ndugga-Kabuye, M.K., Heigham, E., Jayadev, S., Meabon, J.S., Gomez, C.M., Keene, C.D., Cook, D.G., et al., 2020. Heterozygous STUB1 missense variants cause ataxia, cognitive decline, and STUB1 mislocalization. Neurol. Genet. 6, 1–13.

Chen, H.-Y., Hsu, C.-L., Lin, H.-Y., Lin, Y.-F., Tsai, S.-F., Ho, Y.-J., Li, Y.-R., Tsai, J.-W., Teng, S.-C., Lin, C.-H., 2021. Clinical and functional characterization of a novel STUB1 frameshift mutation in autosomal dominant spinocerebellar ataxia type 48 (SCA48). J. Biomed. Sci. 28, 65.

Chiu, H.-H., Hsaio, C.-T., Tsai, Y.-S., Liao, Y.-C., Lee, Y.-C., Soong, B.-W., 2020. Clinical and genetic characterization of autosomal recessive spinocerebellar Ataxia type 16 (SCAR16) in Taiwan. Cerebellum 19, 544–549.

Cordoba, M., Rodriguez-Quiroga, S., Gatto, E.M., Alurralde, A., Kauffman, M.A., 2014. Ataxia plus myoclonus in a 23-year-old patient due to STUB1 mutations. Neurology 83, 287–288.

Cornelissen, T., Vilain, S., Vints, K., Gounko, N., Verstreken, P., Vandenberghe, W., 2018. Deficiency of parkin and PINK1 impairs age-dependent mitophagy in Drosophila. Elife 7.

Coutelier, M., Coarelli, G., Monin, M.-L., Konop, J., Davoine, C.-S., Tesson, C., Valter, R., Anheim, M., Behin, A., Castelnovo, G., et al., 2017. A panel study on patients with dominant cerebellar ataxia highlights the frequency of channelopathies. Brain 140, 1579–1594.

Dai, Q., Zhang, C., Wu, Y., McDonough, H., Whaley, R.A., Godfrey, V., Li, H.-H., Madamanchi, N., Xu, W., Neckers, L., et al., 2003. CHIP activates HSF1 and confers protection against apoptosis and cellular stress. EMBO J. 22, 5446–5458.

De Snoo, M.L., Friesen, E.L., Zhang, Y.T., Earnshaw, R., Dorval, G., Kapadia, M., O'Hara, D.M., Agapova, V., Chau, H., Pellerito, O., et al., 2019. Bcl-2-associated athanogene 5 (BAG5) regulates Parkin-dependent mitophagy and cell death. Cell Death Dis. 10, 1–14.

Depondt, C., Donatello, S., Simonis, N., Rai, M., van Heurck, R., Abramowicz, M., D'Hooghe, M., Pandolfo, M., 2014. Autosomal recessive cerebellar ataxia of adult onset due to STUB1 mutations. Neurology 82, 1749–1750.

Durcan, T.M., Tang, M.Y., Pérusse, J.R., Dashti, E.A., Aguileta, M.A., McLelland, G.-L., Gros, P., Shaler, T.A., Faubert, D., Coulombe, B., et al., 2014. USP8 regulates mitophagy by removing K6-linked ubiquitin conjugates from parkin. EMBO J. 33, 2473–2491.
Fang, E.F., Hou, Y., Palikaras, K., Adriaanse, B.A., Kerr, J.S., Yang, B., Lautrup, S., Hasan-Olive, M.M., Caponio, D., Dan, X., et al., 2019. Mitophagy inhibits amyloid-β and tau pathology and reverses cognitive deficits in models of Alzheimer's disease. Nat. Neurosci. 22, 401–412.
Friesen, E.L., Zhang, Y.T., Earnshaw, R., De Snoo, M.L., O'Hara, D.M., Agapova, V., Chau, H., Ngana, S., Chen, K.S., Kalia, L.V., et al., 2020. BAG5 promotes alpha-synuclein oligomer formation and functionally interacts with the autophagy adaptor protein p62. Front. Cell. Dev. Biol. 8.
Gazulla, J., Izquierdo-Alvarez, S., Sierra-Martínez, E., Marta-Moreno, M.E., Alvarez, S., 2018. Inaugural cognitive decline, late disease onset and novel STUB1 variants in SCAR16. Neurol. Sci. 39, 2231–2233.
Gegg, M.E., Cooper, J.M., Chau, K., Rojo, M., Schapira, A.H.V., 2010. Mitofusin 1 and mitofusin 2 are ubiquitinated in a PINK1 / parkin-dependent manner upon induction of mitophagy. Hum. Mol. Genet. 19, 4861–4870.
Geisler, S., Holmström, K.M., Treis, A., Skujat, D., Weber, S.S., Fiesel, F.C., Kahle, P.J., Springer, W., 2010. The PINK1/Parkin-mediated mitophagy is compromised by PD-associated mutations. Autophagy 6, 871–878.
Genis, D., Ortega-Cubero, S., San Nicolás, H., Corral, J., Gardenyes, J., de Jorge, L., López, E., Campos, B., Lorenzo, E., Tonda, R., et al., 2018. Heterozygous STUB1 mutation causes familial ataxia with cognitive affective syndrome (SCA48). Neurology 91, e1988–e1998.
Grumati, P., Dikic, I., 2018. Ubiquitin signaling and autophagy. J. Biol. Chem. 293, 5404–5413.
Guo, D., Ying, Z., Wang, H., Chen, D., Gao, F., Ren, H., Wang, G., 2015. Regulation of autophagic flux by CHIP. Neurosci. Bull. 31, 469–479.
Harmuth, T., Weber, J.J., Zimmer, A.J., Sowa, A.S., Schmidt, J., Fitzgerald, J.C., Schöls, L., Riess, O., Hübener-Schmid, J., 2022. Mitochondrial dysfunction in spinocerebellar Ataxia type 3 is linked to VDAC1 Deubiquitination. Int. J. Mol. Sci. 23, 5933.
Hayer, S.N., Deconinck, T., Bender, B., Smets, K., Züchner, S., Reich, S., Schöls, L., Schüle, R., De Jonghe, P., Baets, J., et al., 2017. STUB1/CHIP mutations cause Gordon Holmes syndrome as part of a widespread multisystemic neurodegeneration: evidence from four novel mutations. Orphanet J. Rare Dis. 12, 31.
Heimdal, K., Sanchez-Guixé, M., Aukrust, I., Bollerslev, J., Bruland, O., Jablonski, G.E., Erichsen, A.K., Gude, E., Koht, J.A., Erdal, S., et al., 2014. STUB1 mutations in autosomal recessive ataxias - evidence for mutation-specific clinical heterogeneity. Orphanet J. Rare Dis. 9, 146.
Hsieh, C.-H., Shaltouki, A., Gonzalez, A.E., Bettencourt da Cruz, A., Burbulla, L.F., St Lawrence, E., Schüle, B., Krainc, D., Palmer, T.D., Wang, X., 2016. Functional impairment in Miro degradation and Mitophagy is a shared feature in familial and sporadic Parkinson's disease. Cell Stem Cell 19, 709–724.
Imai, Y., Soda, M., Hatakeyama, S., Akagi, T., Hashikawa, T., Nakayama, K.I., Takahashi, R., 2002. CHIP is associated with Parkin, a gene responsible for familial Parkinson's disease, and enhances its ubiquitin ligase activity. Mol. Cell 10, 55–67.
Kalia, L.V., Kalia, S.K., Chau, H., Lozano, A.M., Hyman, B.T., McLean, P.J., 2011. Ubiquitinylation of α-synuclein by carboxyl terminus Hsp70-interacting protein (CHIP) is regulated by Bcl-2-associated athanogene 5 (BAG5). PLoS One 6, e14695.
Kanack, A.J., Newsom, O.J., Scaglione, K.M., 2018. Most mutations that cause spinocerebellar ataxia autosomal recessive type 16 (SCAR16) destabilize the protein quality-control E3 ligase CHIP. J. Biol. Chem. 293, 2735–2743.
Katayama, H., Kogure, T., Mizushima, N., Yoshimori, T., Miyawaki, A., 2011. A sensitive and quantitative technique for detecting Autophagic events based on lysosomal delivery. Chem. Biol. 18, 1042–1052.
Kawarai, T., Miyamoto, R., Shimatani, Y., Orlacchio, A., Kaji, R., 2016. Choreoathetosis, dystonia, and myoclonus in 3 siblings with autosomal recessive spinocerebellar Ataxia type 16. JAMA Neurol. 73, 888–890.
Lee, J.J., Sanchez-Martinez, A., Zarate, A.M., Benincá, C., Mayor, U., Clague, M.J., Whitworth, A.J., 2018. Basal mitophagy is widespread in Drosophila but minimally affected by loss of Pink1 or parkin. J. Cell Biol. 217, 1613–1622.
Lieto, M., Riso, V., Galatolo, D., De Michele, G., Rossi, S., Barghigiani, M., Cocozza, S., Pontillo, G., Trovato, R., Saccà, F., et al., 2020. The complex phenotype of spinocerebellar ataxia type 48 in eight unrelated Italian families. Eur. J. Neurol. 27, 498–505.
Liu, Y.-T., Sliter, D.A., Shammas, M.K., Huang, X., Wang, C., Calvelli, H., Maric, D.S., Narendra, D.P., 2024. Mt-Keima detects PINK1-PRKN mitophagy in vivo with greater sensitivity than mito-QC. Autophagy 17, 3753–3762.
Lizama, B.N., Palubinsky, A.M., McLaughlin, B., 2018. Alterations in the E3 ligases Parkin and CHIP result in unique metabolic signaling defects and mitochondrial quality control issues. Neurochem. Int. 117, 139–155.
Madrigal, S.C., McNeil, Z., Sanchez-Hodge, R., Shi, C., Patterson, C., Scaglione, K.M., Schisler, J.C., 2019. Changes in protein function underlie the disease spectrum in patients with CHIP mutations. J. Biol. Chem. 294, 19236–19245.
Magri, S., Nanetti, L., Gellera, C., Sarto, E., Rizzo, E., Mongelli, A., Ricci, B., Fancellu, R., Sambati, L., Cortelli, P., et al., 2022. Digenic inheritance of STUB1 variants and TBP polyglutamine expansions explains the incomplete penetrance of SCA17 and SCA48. Genet. Med. 24, 29–40.
Martín-Maestro, P., Gargini, R., Perry, G., Avila, J., García-Escudero, V., 2016. PARK2 enhancement is able to compensate mitophagy alterations found in sporadic Alzheimer's disease. Hum. Mol. Genet. 25, 792–806.
Matsuda, N., Sato, S., Shiba, K., Okatsu, K., Saisho, K., Gautier, C.A., Sou, Y., Saiki, S., Kawajiri, S., Sato, F., et al., 2010. PINK1 stabilized by mitochondrial depolarization recruits Parkin to damaged mitochondria and activates latent Parkin for mitophagy. J. Cell Biol.: Report 189, 211–221.
McDonough, H., Patterson, C., 2003. CHIP: a link between the chaperone and proteasome systems. Cell Stress Chaperones 8, 303–308.
McLelland, G.-L., Goiran, T., Yi, W., Dorval, G., Chen, C.X., Lauinger, N.D., Krahn, A.I., Valimehr, S., Rakovic, A., Rouiller, I., et al., 2018. Mfn2 ubiquitination by PINK1/parkin gates the p97-dependent release of ER from mitochondria to drive mitophagy. Elife 7, e32866.
McWilliams, T.G., Prescott, A.R., Allen, G.F.G., Tamjar, J., Munson, M.J., Thomson, C., Muqit, M.M.K., Ganley, I.G., 2016. Mito-QC illuminates mitophagy and mitochondrial architecture in vivo. J. Cell Biol. 214, 333–345.
McWilliams, T.G., Prescott, A.R., Montava-Garriga, L., Ball, G., Singh, F., Barini, E., Muqit, M.M.K., Brooks, S.P., Ganley, I.G., 2018. Basal Mitophagy occurs independently of PINK1 in mouse tissues of high metabolic demand. Cell Metab. 27, 439–449.e5.
Mengel, D., Traschütz, A., Reich, S., Leyva-Gutiérrez, A., Bender, F., Hauser, S., Haack, T. B., Synofzik, M., 2021. A de novo STUB1 variant associated with an early adult-onset multisystemic ataxia phenotype. J. Neurol. 268, 3845–3851.
Michele, G.D., Lieto, M., Galatolo, D., Salvatore, E., Cocozza, S., Barghigiani, M., Tessa, A., Baldacci, J., Pappatà, S., Filla, A., et al., 2019. Spinocerebellar ataxia 48 presenting with ataxia associated with cognitive, psychiatric, and extrapyramidal features: a report of two Italian families. Parkinsonism Relat. Disord. 65, 91–96.
Mol, M.O., van Rooij, J.G.J., Brusse, E., Verkerk, A.J.M.H., Melhem, S., den Dunnen, W.F. A., Rizzu, P., Cupidi, C., van Swieten, J.C., Donker Kaat, L., 2020. Clinical and pathologic phenotype of a large family with heterozygous STUB1 mutation. Neurol. Genet. 6, e417.
Mylvaganam, S., Earnshaw, R., Heymann, G., Kalia, S.K., Kalia, L.V., 2021. C-terminus of Hsp70 interacting protein (CHIP) and neurodegeneration: lessons from the bench and bedside. Curr. Neuropharmacol. 19, 1038–1068.
Olszewska, D.A., Kinsella, J.A., 2020. Extending the phenotypic Spectrum associated with STUB1 mutations: a case of dystonia. Movem. Disord. Clin. Pract. 7, 318–324.
Pakdaman, Y., Sanchez-Guixé, M., Kleppe, R., Erdal, S., Bustad, H.J., Bjørkhaug, L., Haugarvoll, K., Tzoulis, C., Heimdal, K., Knappskog, P.M., et al., 2017. In vitro characterization of six STUB1 variants in spinocerebellar ataxia 16 reveals altered structural properties for the encoded CHIP proteins. Biosci. Rep. 37.
Pakdaman, Y., Denker, E., Austad, E., Norton, W.H.J., Rolfsnes, H.O., Bindoff, L.A., Tzoulis, C., Aukrust, I., Knappskog, P.M., Johansson, S., et al., 2021. Chip protein U-box domain truncation affects Purkinje neuron morphology and leads to behavioral changes in zebrafish. Front. Mol. Neurosci. 14, 723912.
Palikaras, K., Tavernarakis, N., 2017. In vivo Mitophagy monitoring in Caenorhabditis elegans to determine mitochondrial homeostasis. Bio-Protoc. 7, e2215.
Palikaras, K., Lionaki, E., Tavernarakis, N., 2018. Mechanisms of mitophagy in cellular homeostasis, physiology and pathology. Nat. Cell Biol. 20, 1013–1022.
Palomo, G.M., Granatiero, V., Kawamata, H., Konrad, C., Kim, M., Arreguin, A.J., Zhao, D., Milner, T.A., Manfredi, G., 2018. Parkin is a disease modifier in the mutant SOD1 mouse model of ALS. EMBO Mol. Med. 10.
Palubinsky, A.M., Stankowski, J.N., Kale, A.C., Codreanu, S.G., Singer, R.J., Liebler, D.C., Stanwood, G.D., McLaughlin, B., 2015. CHIP is an essential determinant of neuronal mitochondrial stress signaling. Antioxid. Redox Signal. 23, 535–549.
Palvadeau, R., Kaya-Güleç, Z.E., Şimşir, G., Vural, A., Öztop-Çakmak, Ö., Genç, G., Aygün, M.S., Falay, O., Başak, A.N., Ertan, S., 2020. Cerebellar cognitive-affective syndrome preceding ataxia associated with complex extrapyramidal features in a Turkish SCA48 family. Neurogenetics 21, 51–58.
Radziwonik, W., Elert-Dobkowska, E., Klimkowicz-Mrowiec, A., Ziora-Jakutowicz, K., Stepniak, I., Zaremba, J., Sulek, A., 2022. Application of a custom NGS gene panel revealed a high diagnostic utility for molecular testing of hereditary ataxias. J. Appl. Genet. 63, 513–525.
Ravel, J.-M., Benkirane, M., Calmels, N., Marelli, C., Ory-Magne, F., Ewenczyk, C., Halleb, Y., Tison, F., Lecocq, C., Pische, G., et al., 2021. Expanding the clinical spectrum of STIP1 homology and U-box containing protein 1-associated ataxia. J. Neurol. 268, 1927–1937.
Reis, M.C., Patrun, J., Ackl, N., Winter, P., Scheifele, M., Danek, A., Nolte, D., 2022. A severe dementia syndrome caused by intron retention and cryptic splice site activation in STUB1 and exacerbated by TBP repeat expansions. Front. Mol. Neurosci. 15, 878236.
Retterer, K., Juusola, J., Cho, M.T., Vitazka, P., Millan, F., Gibellini, F., Vertino-Bell, A., Smaoui, N., Neidich, J., Monaghan, K.G., et al., 2016. Clinical application of whole-exome sequencing across clinical indications. Genet. Med. 18, 696–704.
Rogers, R.S., Tungtur, S., Tanaka, T., Nadeau, L.L., Badawi, Y., Wang, H., Ni, H.-M., Ding, W.-X., Nishimune, H., 2017. Impaired Mitophagy plays a role in denervation of neuromuscular junctions in ALS mice. Front. Neurosci. 11.
Roux, T., Barbier, M., Papin, M., Davoine, C.-S., Sayah, S., Coarelli, G., Charles, P., Marelli, C., Parodi, L., Tranchant, C., et al., 2020. Clinical, neuropathological, and genetic characterization of STUB1 variants in cerebellar ataxias: a frequent cause of predominant cognitive impairment. Genet. Med. 22, 1851–1862.
Saito, R., Tada, Y., Oikawa, D., Sato, Y., Seto, M., Satoh, A., Kume, K., Ueki, N., Nakashima, M., Hayashi, S., et al., 2022. Spinocerebellar ataxia type 17-digenic TBP/STUB1 disease: neuropathologic features of an autopsied patient. Acta Neuropathol. Commun. 10, 177.
Schisler, J.C., Patterson, C., Willis, M.S., 2016. Skeletal muscle mitochondrial alterations in carboxyl terminus of HSC70 interacting protein (CHIP) −/− mice. Afr. J. Cell Pathol. 6, 28–36.
Sha, Y., Rao, L., Settembre, C., Ballabio, A., Eissa, N.T., 2017. STUB1 regulates TFEB-induced autophagy-lysosome pathway. EMBO J. 36, 2544–2552.

Shi, Y., Wang, J., Li, J.-D., Ren, H., Guan, W., He, M., Yan, W., Zhou, Y., Hu, Z., Zhang, J., et al., 2013. Identification of CHIP as a novel causative gene for autosomal recessive cerebellar ataxia. PLoS One 8, e81884.

Shi, C.-H., Schisler, J.C., Rubel, C.E., Tan, S., Song, B., McDonough, H., Xu, L., Portbury, A.L., Mao, C.-Y., True, C., et al., 2014. Ataxia and hypogonadism caused by the loss of ubiquitin ligase activity of the U box protein CHIP. Hum. Mol. Genet. 23, 1013–1024.

Sun, N., Malide, D., Liu, J., Rovira, I.I., Combs, C.A., Finkel, T., 2017. A fluorescence-based imaging method to measure in vitro and in vivo mitophagy using mt-Keima. Nat. Protoc. 12, 1576–1587.

SunyBiotech, 2024. C.Elegans Gene Editing. https://www.sunybiotech.com/.

Synofzik, M., Schüle, R., Schulze, M., Gburek-Augustat, J., Schweizer, R., Schirmacher, A., Krägeloh-Mann, I., Gonzalez, M., Young, P., Züchner, S., et al., 2014. Phenotype and frequency of STUB1 mutations: next-generation screenings in Caucasian ataxia and spastic paraplegia cohorts. Orphanet J. Rare Dis. 9, 57.

Tang, M.Y., Vranas, M., Krahn, A.I., Pundlik, S., Trempe, J.-F., Fon, E.A., 2017. Structure-guided mutagenesis reveals a hierarchical mechanism of Parkin activation. Nat. Commun. 8, 14697.

Turkgenc, B., Sanlidag, B., Eker, A., Giray, A., Kutuk, O., Yakicier, C., Tolun, A., Temel, S. G., 2018. *STUB1* polyadenylation signal variant AACAAA does not affect polyadenylation but decreases *STUB1* translation causing SCAR16. Hum. Mutat. 39, 1344–1348.

Umano, A., Fang, K., Qu, Z., Scaglione, J.B., Altinok, S., Treadway, C.J., Wick, E.T., Paulakonis, E., Karunanayake, C., Chou, S., et al., 2022. The molecular basis of spinocerebellar ataxia type 48 caused by a de novo mutation in the ubiquitin ligase CHIP. J. Biol. Chem. 298, 101899.

Yamano, K., Youle, R.J., 2013. PINK1 is degraded through the N-end rule pathway. Autophagy 9, 1758–1769.

Ye, X., Sun, X., Starovoytov, V., Cai, Q., 2015. Parkin-mediated mitophagy in mutant hAPP neurons and Alzheimer's disease patient brains. Hum. Mol. Genet. 24, 2938–2951.

Yi, W., MacDougall, E.J., Tang, M.Y., Krahn, A.I., Gan-Or, Z., Trempe, J.-F., Fon, E.A., 2019. The landscape of Parkin variants reveals pathogenic mechanisms and therapeutic targets in Parkinson's disease. Hum. Mol. Genet. 28, 2811–2825.

Yoo, L., Chung, K.C., 2018. The ubiquitin E3 ligase CHIP promotes proteasomal degradation of the serine/threonine protein kinase PINK1 during staurosporine-induced cell death. J. Biol. Chem. 293, 1286–1297.

Youle, R.J., Narendra, D.P., 2011. Mechanisms of mitophagy. Nature 12, 9–13.

Zhang, B., Hu, Z., Yin, X., Cai, M., Zhao, G., Liu, Z., Luo, W., 2010. Mutation analysis of parkin and PINK1 genes in early-onset Parkinson's disease in China. Neurosci. Lett. 477, 19–22.

Zhang, N., Hi, W., Dg, C., Burchell, L., Walden, H., Tj, M., Deak, M., Knebel, A., Pink, M. M.M.K., Kondapalli, C., et al., 2012. PINK1 Is Activated by Mitochondrial Membrane Potential Depolarization and Stimulates Parkin E3 Ligase Activity by Phosphorylating Serine 65. Open Biology.